Optical spin- and current-injection and second harmonic generation study on hydrogenated graphene structures

Reinaldo A. Zapata, Sean M. Anderson, and Bernardo S. Mendoza

Centro de Investigaciones en Optica, A.C.

Anatoli I. Shkrebtii

Department of Physics, University of Toronto

Lorem ipsum dolor sit amet, consectetuer adipiscing elit. Etiam lobortis facilisis sem. Nullam nec mi et neque pharetra sollicitudin. Praesent imperdiet mi nec ante. Donec ullamcorper, felis non sodales commodo, lectus velit ultrices augue, a dignissim nibh lectus placerat pede. Vivamus nunc nunc, molestie ut, ultricies vel, semper in, velit. Ut porttitor. Praesent in sapien. Lorem ipsum dolor sit amet, consectetuer adipiscing elit. Duis fringilla tristique neque. Sed interdum libero ut metus. Pellentesque placerat. Nam rutrum augue a leo. Morbi sed elit sit amet ante lobortis sollicitudin. Praesent blandit blandit mauris. Praesent lectus tellus, aliquet aliquam, luctus a, egestas a, turpis. Mauris lacinia lorem sit amet ipsum. Nunc quis urna dictum turpis accumsan semper.

I.   INTRODUCTION

Graphene is an allotrope of carbon with a planar hexagonal two-dimensional honeycomb structure or equilateral triangular crystal lattice in which one carbon atom occupies a vertex [1]. In 2010 Geim and Novoselov received the Nobel Prize for the research of properties about this material [1]. Some of the properties of graphene are mechanical strength, optical absorption coefficient and thermal conductivity [1, 2]. Also graphene behaves like a metal [1] but it presents a tunable band gap by changing the layer surface [3], aplying an electric field [4], and doping [5–8]. As shown in Figure 1 when a hydrogen is bonded to a carbon atom from graphene structure, it pulls the carbon atom modifying the carbon–carbon bond length in the planar structure and then opening the gap [8]. The structures presented in this paper are hydrogenated graphene structures presenting a gap of energy.

In this paper, we are focused in the characterization of three phenomena of interest, all of them recently studied on semiconducting bulk an surfaces systems: the one-photon optical spin- and current-injection and second harmonic generation (SHG). First, the optical spin-injection might be characterized by the physical dimensionless quantity of degree of spin polarization (DSP), in the i direction (D^i), which is a function of the photon frequency, ω. The DSP gives a quantitative value of the fraction of injected electrons from the valence to the conduction bands that are spin polarized. There are theoretical reports of calculations for the spin injection in bulk media (Si, GaAs, CdSe, and Ge semiconductors) [9–11] and surfaces [Si(111):In, Si(111):As, GaAs(110):Sb, GaAs(110), and Si(111) with 4×2 and 8×2 reconstructions][12, 13]. Hereupon, the one-photon current injection is characterized by the current injection tensor, $\eta(0; \omega, -\omega)$ being a particular case of the current injection tensor $\eta(\omega_1 - \omega_2; \omega_1, -\omega_2)$, where $\omega 1$ and $\omega 2$ are the frequencies of two different incident beams. The frequency dependence of the injection current tensor is expressed as $\eta(\omega)$ instead of $\eta(0; \omega, -\omega)$.

In the other hand, nonlinear optical spectroscopies, particularly SHG, are important methods to study surfaces. The importance of this kind of tests come from their noninvasive and nondestructive nature to study surfaces and interfaces obtaining as result the atomic structure, phase transitions, adsorption of atoms, and many other properties [14–21]. For the calculation of the SHG we followed the new formalism developed by Anderson *et al.* for theoretical approach of surface second-harmonic generation from semiconductor surfaces [22] based on the $\mathbf{r} \cdot \mathbf{E}$ or *length gauge* and the electron density operator. This formalism can be applied to surface and bulk structures [22, 23].

The sections organization of this paper is as follows. In Sec. II we present the theory that describes the DSP and current injection, in a given i direction, D^i, η^{ijk}, and the SHG. The description of those phenomena are given in the independent-particle approximation. In Sec. III we describe the details of the calculation for the responses and the corresponding spectra for D^i, η^{ijk}, and SHG for the respective *alt* and *up* structures. Finally, we give conclusions in Sec. IV.

II.   THEORY

A.   Optical spin injection

The injection and detection of spin polarized electrons into nonmagnetic materials is the core of spintronics [24–28] and an important problem in condensed matter. The process of optical spin injection of carriers appears when circularly polarized light [29] insides in a semiconductor media promoting spin-polarized electrons from the valence to the conduction bands. This process takes place as a result of the interaction of electron spin and motion caused by the spin-orbit
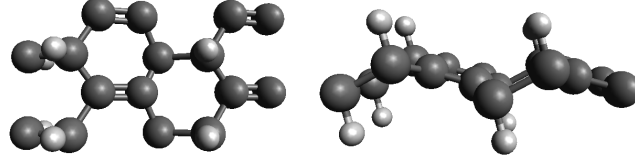
(a)
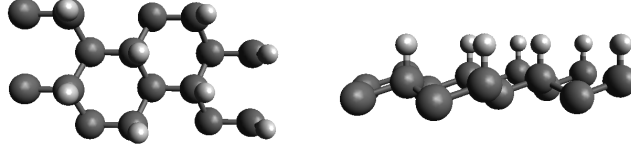
(b)

FIG. 1. Top and side views of the [1(a)] $C_{16}H_8$-alt and [1(b)] $C_{16}H_8$-up structures. The dark and light spheres correspond to carbon and hydrogen atoms, respectively.

coupling in media. The DSP gives a quantitative value of the fraction of injected electrons into the conduction bands that are spin polarized. It can be calculated by full band structure local-density approximation (LDA) and $\mathbf{k} \cdot \mathbf{p}$ methods [9, 10].

Mendoza and Cabellos derived the expressions for the optical spin generation suitable for surfaces and interfaces [12]. They used a slab approach in order to model the surface. They wrote the surface DSP along direction i as

$$D^i(\omega) = \frac{-2i\zeta^{ixy}(\omega)}{\hbar \left[\xi^{xx}(\omega) + \xi^{yy}(\omega)\right]/2} \tag{1}$$

where $\zeta^{ixy}(\omega)$ and $\xi^{aa}(\omega)$ are the surface spin-injection rate tensor components and are diagonal components of the surface carrier generation rate tensor, respectively, and the indexes i,j,k denote Cartesian coordinates.

In our calculation we consider a normal incidence of circularly polarized light propagating along the -z direction,

$$\mathbf{E}(\omega) = E_0(\hat{x} - i\hat{y})/\sqrt{2},$$

where E_0 is the field intensity. Taking in account that there is possible to generate spin-polarized electrons, from the valence to the conduction bands, along the $\hat{i}$, $\hat{j}$, and $\hat{k}$ directions with incident light on the surface plane, the total DSP can be obtained by the relation

$$|D^{\mathrm{T}}| = \sqrt{[D^x]^2 + [D^y]^2 + [D^z]^2}$$

where the dependence in frequency, ω, has been omitted.

B. Optical current injection

The optical current injection is a second-order nonlinear effect that takes place in non-centrosymmetric structures [30–33]. The photocurrent can be injected with a single optical beam and is produced by the interference of one photon-absorption processes associated with different linear polarizations of light [23]. Also called *circular photovoltaic effect* the optical current injection occurs in a non-centrosymmetric media when it is photoexcited with circularly polarized light, producing an interference effect in the excitation pathways, and resulting in an asymmetric population of the injected carriers in reciprocal space and, therefor, a photocurrent. This photocurrent phenomena has been studied in bulk semiconductors, one dimensional (1D) nanotubes [34, 35], and two dimensional (2D) surfaces [34].

In the year 2011 Cabellos and Mendoza *et al.* [31] derived the expression for the generation of the injection current for surfaces and interfaces. They defined the surface injection current as

$$\dot{\mathbf{J}}^i_{\text{inj}}(\omega) = \eta^{ijk}(\omega) E_j(\omega) E_k(\omega), \tag{2}$$

where $\eta^{ijk}(\omega)$ is the surface injection current tensor. Thus, according to Eq. 2, a photocurrent is optically injected in the direction i when two polarized electric fields, in the j and k directions, inside over a surface. For a surface system we have that η^{ixy} is given by [13, 31]

$$\eta^{ijk}(\omega) = \ell_{\text{eff}} \times \sum_{\ell=1}^{n_{eff}} \eta_{ijk}(\ell|\omega). \tag{3}$$

where the sum is made over the number of layers that contributes to the response of the media, $\eta_{ijk}(\ell|\omega)$ corresponds to the ℓ_{th}-layer contribution to the surface injection current tensor and ℓ_{eff} is the thickness to the total layers that contribute to the response. The tensor $\eta^{ijk}(\omega)$ is purely imaginary and has the property of being antisymmetric in the last two Cartesian indices, j and k [23, 30].

Taking in account that with circularly polarized light it is possible to generate current injection along the $\hat{i}$, $\hat{j}$, and $\hat{k}$ directions with incident light on the surface plane, the total injection current can be obtained in a similar way as has been done in 1

$$|\eta^{\text{T}}| = \sqrt{[\eta^{xxy}]^2 + [\eta^{yxy}]^2 + [\eta^{zxy}]^2}$$

where the dependence in frequency, ω, has been omitted again.

The units of both $\dot{\mathbf{J}}^i_{\text{inj}}(\omega)$ and $\eta^{ijk}(\omega)$ are those of their bulk equivalents times ℓ_{eff} expressed in the corresponding units to report [31].

C. Second harmonic generation

SHG, also called frequency doubling, is a particular case of the nonlinear optical process of sum of frequency in which photons of same frequency are annihilated to produce a new photon with twice frequency, energy and half of wavelength of the initial photons. This phenomena occurs when light beams from coherent sources inside over a nonlinear media that does not present inversion of symmetry [19, 22, 23, 36].

Recently, Anderson *et al.* [22] developed a new formalism to calculate the second order susceptibility which includes the scissors correction, needed to have the correct value of the energy

band gap; the contribution of the nonlocal part of the pseudopotentials, routinely used in ab initio band-structure calculations; and the derivation for the inclusion of the cut function, used to extract the surface response. According to that we have the expressions for the imaginary part of the interband contributions (i) and intraband (e) for 1ω and 2ω

$$\mathrm{Im}[\chi_{e,\omega}^{\mathrm{abc}}] = \frac{\pi|e|^3}{2\hbar^2} \int \frac{dk^3}{8\pi^3} \sum_{vc} \sum_{q\neq(v,c)} \frac{1}{\omega_{cv}^{\Sigma}} \left[\frac{\mathrm{Im}[\mathcal{V}_{qc}^{\Sigma,\mathrm{a}}\{r_{cv}^{\mathrm{b}}r_{vq}^{\mathrm{c}}\}]}{(2\omega_{cv}^{\Sigma} - \omega_{cq}^{\Sigma})} - \frac{\mathrm{Im}[\mathcal{V}_{vq}^{\Sigma,\mathrm{a}}\{r_{qc}^{\mathrm{c}}r_{cv}^{\mathrm{b}}\}]}{(2\omega_{cv}^{\Sigma} - \omega_{qv}^{\Sigma})} \right] \delta(\omega_{cv}^{\Sigma} - \omega), \quad (4\mathrm{a})$$

$$\mathrm{Im}[\chi_{i,\omega}^{\mathrm{abc}}] = \frac{\pi|e|^3}{2\hbar^2} \int \frac{dk^3}{8\pi^3} \sum_{cv} \frac{1}{(\omega_{cv}^{\Sigma})^2} \left[\mathrm{Re}\left[\left\{ r_{cv}^{\mathrm{b}}\left(\mathcal{V}_{vc}^{\Sigma,\mathrm{a}}\right)_{;k^{\mathrm{c}}}\right\}\right] + \frac{\mathrm{Re}\left[\mathcal{V}_{vc}^{\Sigma,\mathrm{a}}\{r_{cv}^{\mathrm{b}}\Delta_{cv}^{\mathrm{c}}\}\right]}{\omega_{cv}^{\Sigma}} \right] \delta(\omega_{cv}^{\Sigma} - \omega), \quad (4\mathrm{b})$$

$$\mathrm{Im}[\chi_{e,2\omega}^{\mathrm{abc}}] = -\frac{\pi|e|^3}{2\hbar^2} \int \frac{dk^3}{8\pi^3} \sum_{vc} \frac{4}{\omega_{cv}^{\Sigma}} \left[\sum_{v'\neq v} \frac{\mathrm{Im}[\mathcal{V}_{vc}^{\Sigma,\mathrm{a}}\{r_{cv'}^{\mathrm{b}}r_{v'v}^{\mathrm{c}}\}]}{2\omega_{cv'}^{\Sigma} - \omega_{cv}^{\Sigma}} - \sum_{c'\neq c} \frac{\mathrm{Im}[\mathcal{V}_{vc}^{\Sigma,\mathrm{a}}\{r_{cc'}^{\mathrm{c}}r_{c'v}^{\mathrm{b}}\}]}{2\omega_{c'v}^{\Sigma} - \omega_{cv}^{\Sigma}} \right] \delta(\omega_{cv}^{\Sigma} - 2\omega),$$
$$(4\mathrm{c})$$

$$\mathrm{Im}[\chi_{i,2\omega}^{\mathrm{abc}}] = \frac{\pi|e|^3}{2\hbar^2} \int \frac{dk^3}{8\pi^3} \sum_{vc} \frac{4}{(\omega_{cv}^{\Sigma})^2} \left[\mathrm{Re}\left[\mathcal{V}_{vc}^{\Sigma,\mathrm{a}}\left\{\left(r_{cv}^{\mathrm{b}}\right)_{;k^{\mathrm{c}}}\right\}\right] - \frac{2\mathrm{Re}\left[\mathcal{V}_{vc}^{\Sigma,\mathrm{a}}\{r_{cv}^{\mathrm{b}}\Delta_{cv}^{\mathrm{c}}\}\right]}{\omega_{cv}^{\Sigma}} \right] \delta(\omega_{cv}^{\Sigma} - 2\omega).$$
$$(4\mathrm{d})$$

Here, the factor of 2 for spin degeneracy is not included and the real part of each contribution can be obtained through a Kramers-Kronig transformation [37] and

$$\chi^{abc} = \chi_{e,\omega}^{abc} + \chi_{e,2\omega}^{abc} + \chi_{i,\omega}^{abc} + \chi_{i,2\omega}^{abc}. \tag{5}$$

As made before, in Eq. 4 and 5 the dependence in frequency, ω, has been omitted. For our case in Eq. 4, the expression $\mathcal{V}^{\Sigma}$ corresponds to the sum of the LDA and non-local velocity matrix elements, r^{a} are the position matrix elements and $\Delta_{nm}^a = v_{nn}^{\mathrm{LDA},a} - v_{mm}^{\mathrm{LDA},a}$. To accomplish the required intrinsic permutation symmetry, the $\{\}$ notation symmetrizes the bc Cartesian indices, i.e., $\{u^b s^c\} = (u^b s^c + u^c s^b)/2$ and so, $\chi^{abc} = \chi^{acb}$. The units of χ^{ijk}, again, are those of their bulk equivalents times ℓ_{eff} expressed in the corresponding units to report. For full details read the appendix of Ref. [22].

III. RESULTS

We present the results of the numerical calculations for D^a, η^{ixy}, and SHG for the hydrogenated graphene structures, $C_{16}H_8$-alt and $C_{16}H_8$-up shown in Fig. 1. Both structures are infinite carbon planes in an hexagonal honeycomb lattice with %50 of hydrogenation in two different arrangements: the *alt* structure [Fig 1(a)] has alternating hydrogen bonds in the top and bottom sides of the carbon plane; the *up* structure [Fig 1(b)] has hydrogen bonds only in the top side. Both structures are non-centrosymmetric and has a thickness of 5.56 and 2.76 Angstroms, respectively. A vacuum length at least five times the thickness for each structure was taken to construct the super-cell.

In this work we used the ABINIT code [38] for the calculation of the self-consistent ground state and their Kohn-Sham states using DFT-LDA in the plane waves approximation. Also, to
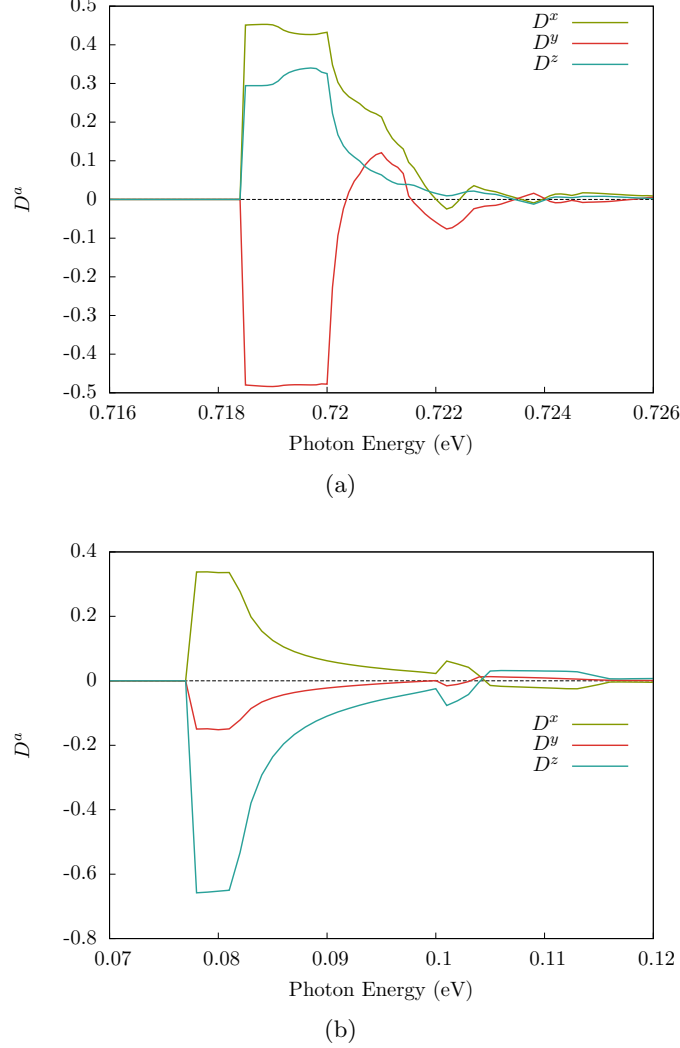
FIG. 2. (Color online) Spectra of the degree of spin polarization along the direction i, D^a, for the hydrogenated graphene structures $C_{16}H_8$-alt [Fig. 2(a)] and $C_{16}H_8$-up [Fig. 2(b)] under incidence of circularly polarized light.

compute the DSP and the optical current injection we used the relativistic separable dual-space Gaussian pseudopotentials of Hartwigsen-Goedecker-Hutter (HGH) [39] including the spin-orbit interaction, necessary to make the calculations of D^i but not in the cases of η^{ixy}. For the caso of SHG Troullier-Martins pseudopotentials [40] that are fully separable nonlocal pseudopotentials in the Kleiman-Bylander form [41]. The contribution of the non-local potential in Eq. 4 is carried out using the DP code [42]. Moreover, we have taken a cutoff energy of 65 and 40 Ha for the *alt* and *up* structures, respectively, and the energy eigenvalues and matrix elements were calculated using 14452 and 8452 **k** points in the irreducible Brillouin zone (IBZ).

In Figs. 2(a) and 2(b) we show the spectra obtained for D^a of the $C_{16}H_8$-alt and $C_{16}H_8$-up structures, respectively. Values over (under) zero define a positive (negative) direction of spin polarization along the a direction. It can be observed that for both structures we have more than 40% of D^a and a maximum absolute value in the y direction, reaching almost a 50% in the *alt* structure. In table I we show a comparison of the maximum degree of spin polarization reported for different structures.To report the η^{ixy} we took in account that our structures are infinite carbon-
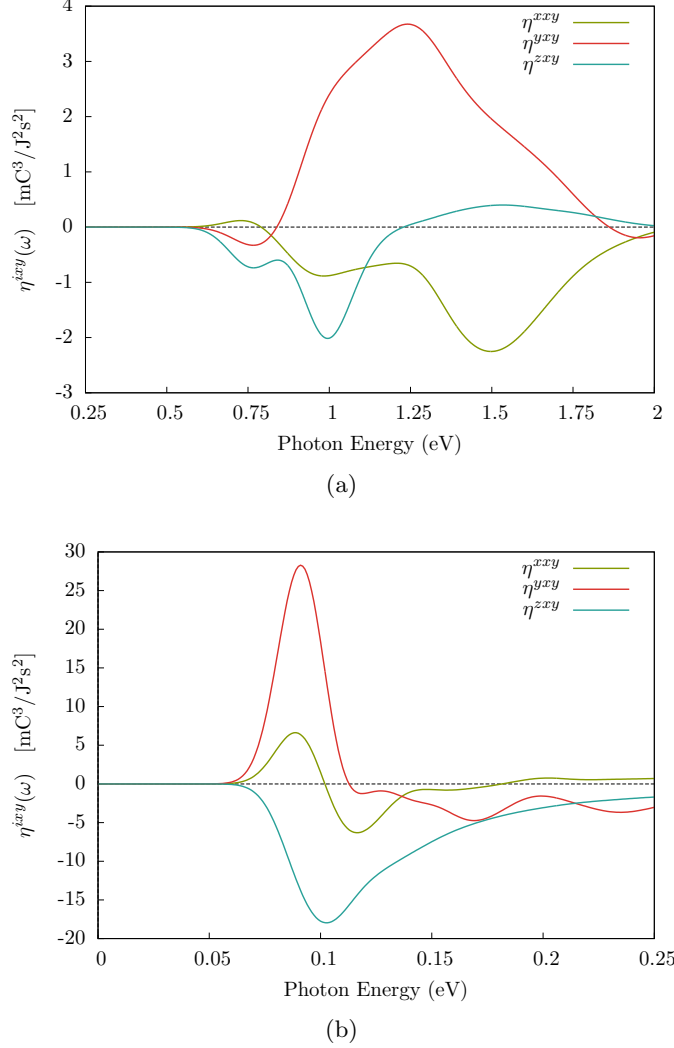
FIG. 3. (Color online) Spectra of the injection current tensor along the direction i, η^{ixy}, for the hydrogenated graphene structures $C_{16}H_8$-alt [Fig 3(a)] and $C_{16}H_8$-up [Fig. 3(b)] under incidence of circularly polarized light.

hydrogen layers. So in Eq. 3 we defined the ℓ_{eff} as the thickness of each structure, 5.56 and 2.76 Angstroms for the *alt* and *up* structures.

We show in Figs. 3(a) and 3(b) the spectra obtained for the current tensor η^{ixy} of the structures *alt* and *up*, respectively. We can observe that circularly polarized light on the plane xy produces injection current along three directions. Values over (under) zero define a positive (negative) direction of current injection along the *a* direction. From Fig. 3 we can see that for the *alt* structure spectra [Fig. 3(a)] we have a positive maximum in the y direction for an incident beam energy of 1.25 eV, reaching a value of $3.7\,\mathrm{mC^3/J^2s^2}$. Also, for the *up* structure spectra [Fig. 3(b)] we have a negative maximum in the x direction for an incident beam energy of 0.405 eV, reaching a value of $3.5\,\mathrm{mC^3/J^2s^2}$. In table II we present a comparison of the maximum current injection reported for different structures.
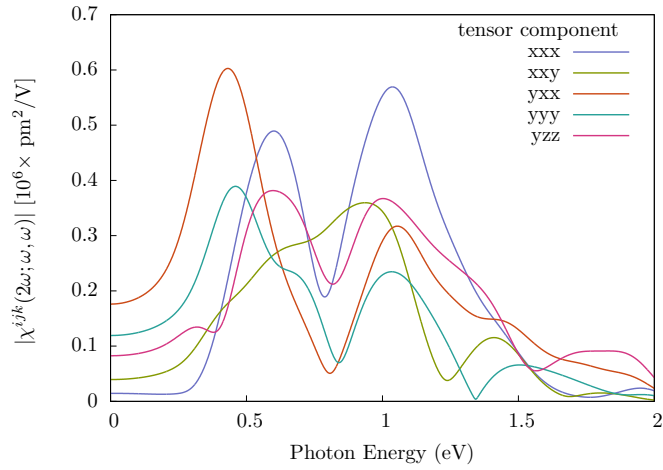
In Figs. 4 and 5 we show the spectra obtained for the SHG for the *alt* and *up* structures, respectively. The Figs. 4(a) and 5(a) show the real part of the non-zero components, Figs. 4(b) and 5(b) the imaginary part, and Figs. 4(c) and 4(c) the absolute value of the $\chi^{ijk}(2\omega;\omega\omega)$ tensor.
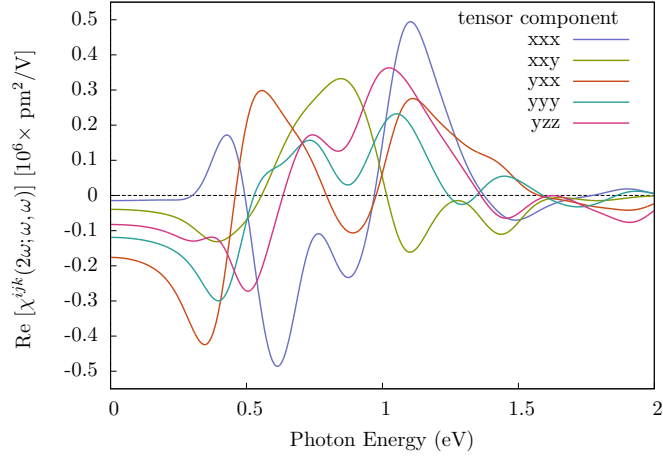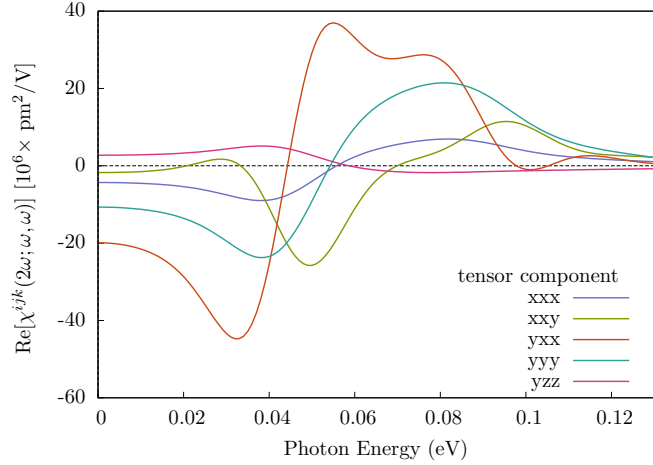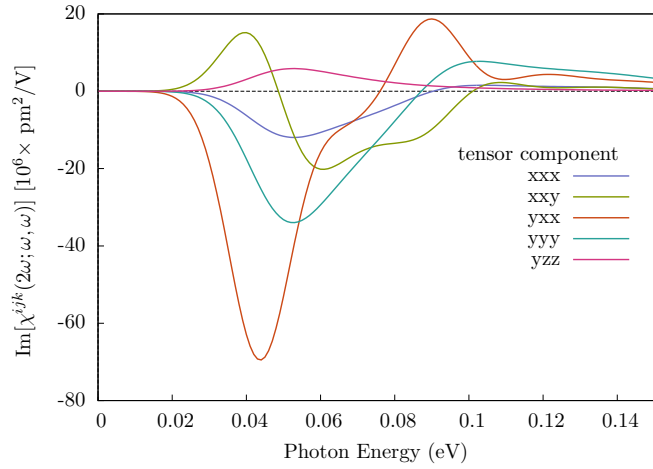
(a)
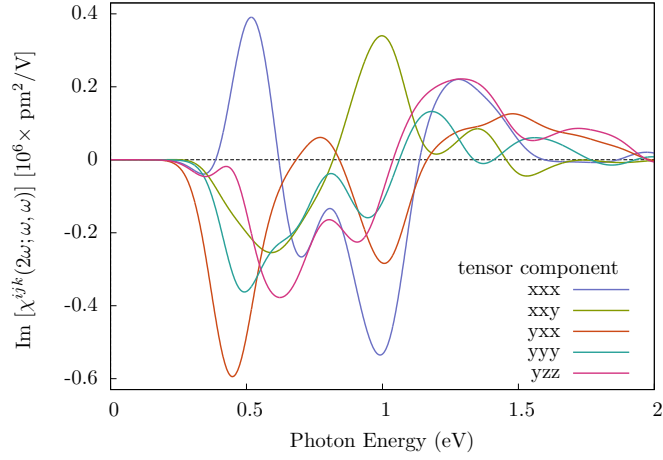
(b)

(c)

FIG. 4. (Color online) Spectra of the SHG for the $C_{16}H_8$-alt structure. The Fig. 4(c) corresponds to the sum of the absolute value for the non zero real [Fig. 4(a)] and imaginary [Fig. 4(b)] components of $\chi^{ijk}(2\omega;\omega,\omega)$ tensor.
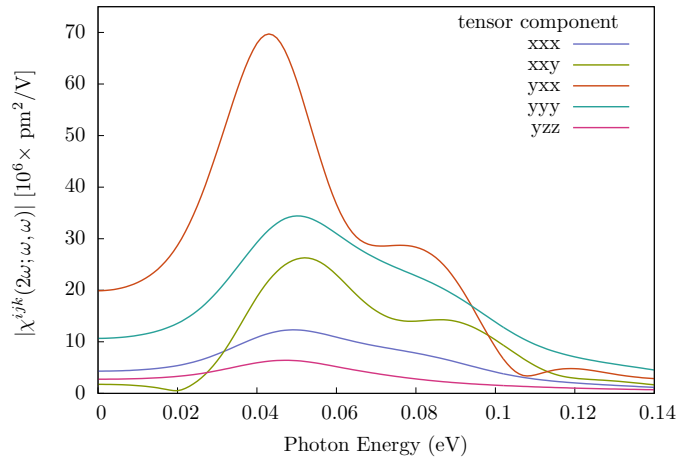
FIG. 5. (Color online) Spectra of the SHG for the $C_{16}H_8$-up structure. The Fig. 5(c) corresponds to the sum of the absolute value for the non zero real [Fig. 5(a)] and imaginary [5(b)] components of $\chi^{ijk}(2\omega;\omega,\omega)$ tensor.

TABLE I. Comparison of the reported absolute values for the highest percentage of D^a for different structures. (*This work.)

Structure	Energy	D^a	Reference
	[eV]	a, [%]	
$C_{16}H_8$-alt	0.719	y, 48	*
$C_{16}H_8$-up	0.40	y, 42	*
Si(111)-In 8×2	0.74	z, 32	[13]
Si(111)-As 1×1	2.20	z, 100	[12]
Bulk Si	3.44	z, 30	[9]

TABLE II. Comparison of the highest reported absolute values of η^{ixy} for different structures. (*This work.)

Structure	Energy	η^{ixy}	Ref.
	[eV]	a, $[\mathrm{mC^3/J^2s^2}]$	
$C_{16}H_8$-alt	1.25	y, 3.70	*
$C_{16}H_8$-up	0.405	x, 3.50	*
Si(111)-In 8×2	1.24	y, 0.35	[13]
Si(111) 2×1	0.75	y, 1.22	[12]
GaAs(110) clean	4.30	y, 0.30	[9]

We can see from Fig. 4 that for the *alt* structure an absolute maximum of the SHG spectra is reached at 0.4 eV with a value of 0.6×10^6 pm^2/V for the χ^{yxx} component produced principally for contributions of the imaginary part. Also, a second local maximum is reached at 1.1 eV with a value of 0.55×10^6 pm^2/V for the χ^{xxx} component having in this case a principal contribution from the real part. Also, from Fig. 5 we can see that for the *up* structure an absolute maximum is reached near to 0.042 eV reaching a value of 70×10^6 pm^2/V for the χ^{yxx} tensor component which contribution comes from the imaginary part of the spectra. In table III we show a comparison of the maximum SHG reported for different structures.

IV.   CONCLUSIONS

Lorem ipsum dolor sit amet, consectetuer adipiscing elit. Etiam lobortis facilisis sem. Nullam nec mi et neque pharetra sollicitudin. Praesent imperdiet mi nec ante. Donec ullamcorper, felis non sodales commodo, lectus velit ultrices augue, a dignissim nibh lectus placerat pede. Vivamus nunc nunc, molestie ut, ultricies vel, semper in, velit. Ut porttitor. Praesent in sapien. Lorem ipsum dolor sit amet, consectetuer adipiscing elit. Duis fringilla tristique neque. Sed interdum libero ut metus. Pellentesque placerat. Nam rutrum augue a leo. Morbi sed elit sit amet ante lobortis

TABLE III. Comparison of the highest reported absolute values of SHG for different structures. (*This work.)

Structure	Energy	χ^{ijk}	Ref.
	[eV]	ijk, $[10^6 \times \mathrm{pm^2/V}]$	
$C_{16}H_8$-alt	1.25	y, 3.70	*
$C_{16}H_8$-up	0.405	x, 3.50	*

sollicitudin. Praesent blandit blandit mauris. Praesent lectus tellus, aliquet aliquam, luctus a, egestas a, turpis. Mauris lacinia lorem sit amet ipsum. Nunc quis urna dictum turpis accumsan semper.

V.   ACKNOWLEDGMENT

[1] A. Geim and K. Novoselov, Nature Materials **6**, 183 (2007).
[2] R. Nair, P. Blake, A. Grigorenko, K. Novoselov, T. Booth, T. Stauber, N. Peres, and A. Geim, Science **320**, 1308 (2008).
[3] M. Han, B. Özyilmaz, Y. Zhang, and P. Kim, Physical Review Letters **98**, 206805 (2007).
[4] Y. Zhang, T. Tang, C. Girit, Z. Hao, M. Martin, A. Zettl, M. Crommie, Y. Shen, and F. Wang, Nature **459**, 820 (2009).
[5] T. Ohta, A. Bostwick, T. Seyller, K. Horn, and E. Rotenberg, Science **313**, 951 (2006).
[6] D. Elias, R. Nair, T. Mohiuddin, S. Morozov, P. Blake, M. Halsall, A. Ferrari, D. Boukhvalov, M. Katsnelson, A. Geim, et al., Science **323**, 610 (2009).
[7] N. Guisinger, G. Rutter, J. Crain, P. First, and J. Stroscio, Nano letters **9**, 1462 (2009).
[8] D. Samarakoon and X. Wang, ACS nano **4**, 4126 (2010).
[9] F. Nastos, J. Rioux, M. Strimas-Mackey, B. S. Mendoza, and J. Sipe, Physical Review B **76**, 205113 (2007).
[10] J. Cabellos, C. Salazar, and B. S. Mendoza, Physical Review B **80**, 245204 (2009).
[11] J. Rioux and J. Sipe, Physical Review B **81**, 155215 (2010).
[12] B. S. Mendoza and J. Cabellos, Physical Review B **85**, 165324 (2012).
[13] N. Arzate, R. Vázquez-Nava, and B. S. Mendoza, Physical Review B **90**, 205310 (2014).
[14] J. Dadap, Z. Xu, X. Hu, M. Downer, N. Russell, J. Ekerdt, and O. Aktsipetrov, Physical Review B **56**, 13367 (1997).
[15] W. Daum, H.-J. Krause, U. Reichel, and H. Ibach, Physical review letters **71**, 1234 (1993).
[16] J. F. McGilp, M. Cavanagh, J. R. Power, and J. D. O'Mahony, Optical Engineering **33**, 3895 (1994).
[17] J. Power, J. O'Mahony, S. Chandola, and J. McGilp, Physical review letters **75**, 1138 (1995).
[18] P. Godefroy, W. De Jong, C. Van Hasselt, M. Devillers, and T. Rasing, Applied physics letters **68**, 1981 (1996).
[19] R. V. Salazar-Aparicio, R. Vázquez-Nava, N. Arzate, and B. S. Mendoza, Physical Review B **90**, 155403 (2014).
[20] C. Chen, A. De Castro, and Y. Shen, Physical Review Letters **46**, 145 (1981).
[21] B. S. Mendoza, A. Gaggiotti, and R. Del Sole, Physical review letters **81**, 3781 (1998).
[22] S. M. Anderson, N. Tancogne-Dejean, B. S. Mendoza, and V. Véniard, Physical Review B **91**, 075302 (2015).
[23] J. Sipe and A. Shkrebtii, Physical Review B **61**, 5337 (2000).
[24] I. Žutić, J. Fabian, and S. D. Sarma, Reviews of modern physics **76**, 323 (2004).
[25] A. Fert, Reviews of Modern Physics **80**, 1517 (2008).
[26] F. Pezzoli, F. Bottegoni, D. Trivedi, F. Ciccacci, A. Giorgioni, P. Li, S. Cecchi, E. Grilli, Y. Song, M. Guzzi, et al., in *SPIE NanoScience+ Engineering* (International Society for Optics and Photonics, 2012), pp. 84610P–84610P.
[27] F. Bottegoni, A. Ferrari, G. Isella, M. Finazzi, and F. Ciccacci, Physical Review B **88**, 121201 (2013).
[28] F. Bottegoni, A. Ferrari, S. Cecchi, M. Finazzi, F. Ciccacci, and G. Isella, Applied Physics Letters **102**, 152411 (2013).
[29] M. Dyakonov and V. Perel, in *Optical orientation* (1984).
[30] F. Nastos and J. Sipe, Physical Review B **74**, 035201 (2006).
[31] J. Cabellos, B. S. Mendoza, and A. Shkrebtii, Physical Review B **84**, 195326 (2011).
[32] R. Bhat and J. Sipe, Physical Review B **72**, 075205 (2005).
[33] J. Fraser, A. Shkrebtii, J. Sipe, and H. Van Driel, Physical review letters **83**, 4192 (1999).

[34] E. J. Mele, P. Král, and D. Tománek, Physical Review B **61**, 7669 (2000).
[35] P. Král, E. Mele, and D. Tománek, Physical review letters **85**, 1512 (2000).
[36] N. Bloembergen and P. Pershan, Physical Review **128**, 606 (1962).
[37] N. Tancogne-Dejean, B. S. Mendoza, and V. Véniard, Physical Review B **90**, 035212 (2014).
[38] M. Torrent, F. Jollet, F. Bottin, G. Zérah, and X. Gonze, Computational Materials Science **42**, 337 (2008).
[39] C. Hartwigsen, S. Gœdecker, and J. Hutter, Physical Review B **58**, 3641 (1998).
[40] N. Troullier and J. L. Martins, Physical review B **43**, 1993 (1991).
[41] L. Kleinman and D. Bylander, Physical Review Letters **48**, 1425 (1982).
[42] V. Olevano, L. Reining, and F. Sottile, http://etsf.polytechnique.fr/Software/Ab_Initio.